Biogeosciences Discuss., 11, 16703–16742, 2014
www.biogeosciences-discuss.net/11/16703/2014/
doi:10.5194/bgd-11-16703-2014

Biogeosciences Discussions
Open Access

Oceanic N_2O emissions in the 21st century

J. Martinez-Rey[1], L. Bopp[1], M. Gehlen[1], A. Tagliabue[2], and N. Gruber[3]

[1]Laboratoire des Sciences du Climat et de l'Environnement, IPSL, CEA/CNRS/UVSQ, Bat. 712, Orme des Merisiers, 91191 CE Saclay, Gif-sur-Yvette, France
[2]School of Environmental Sciences, University of Liverpool, 4 Brownlow Street, Liverpool L69 3GP, UK
[3]Environmental Physics, Institute of Biogeochemistry and Pollutant Dynamics, ETH, CHN E31.2, Universitaetstrasse 16, 8092 Zürich, Switzerland

Received: 16 September 2014 – Accepted: 15 October 2014 – Published: 4 December 2014

Correspondence to: J. Martinez-Rey (jorge.martinez-rey@lsce.ipsl.fr)

Published by Copernicus Publications on behalf of the European Geosciences Union.

Abstract

The ocean is a substantial source of nitrous oxide (N_2O) to the atmosphere, but little is known on how this flux might change in the future. Here, we investigate the potential evolution of marine N_2O emissions in the 21st century in response to anthropogenic climate change using the global ocean biogeochemical model NEMO-PISCES. We implemented two different parameterizations of N_2O production, which differ primarily at low oxygen (O_2) conditions. When forced with output from a climate model simulation run under the business-as-usual high CO_2 concentration scenario (RCP8.5), our simulations suggest a decrease of 4 to 12 % in N_2O emissions from 2005 to 2100, i.e., a reduction from 4.03/3.71 to 3.54/3.56 $Tg\,N\,yr^{-1}$ depending on the parameterization. The emissions decrease strongly in the western basins of the Pacific and Atlantic oceans, while they tend to increase above the Oxygen Minimum Zones (OMZs), i.e., in the Eastern Tropical Pacific and in the northern Indian Ocean. The reduction in N_2O emissions is caused on the one hand by weakened nitrification as a consequence of reduced primary and export production, and on the other hand by stronger vertical stratification, which reduces the transport of N_2O from the ocean interior to the ocean surface. The higher emissions over the OMZ are linked to an expansion of these zones under global warming, which leads to increased N_2O production associated primarily with denitrification. From the perspective of a global climate system, the averaged feedback strength associated with the projected decrease in oceanic N_2O emissions amounts to around $-0.009\,W\,m^{-2}\,K^{-1}$, which is comparable to the potential increase from terrestrial N_2O sources. However, the assesment for a compensation between the terrestrial and marine feedbacks calls for an improved representation of N_2O production terms in fully coupled next generation of Earth System Models.

BGD
11, 16703–16742, 2014

1 Introduction

Nitrous oxide (N_2O) is a gaseous compound responsible for two key feedback mechanisms within the Earth's climate. First, it acts as a long-lived and powerful greenhouse gas (Prather et al., 2012) ranking third in anthropogenic radiative forcing after carbon dioxide (CO_2) and methane (CH_4) (Myrhe et al., 2013). Secondly, the ozone (O_3) layer depletion in the future might be driven mostly by N_2O after the drastic reductions in CFCs emissions start to show their effect on stratospheric chlorine levels (Ravishankara et al., 2009). The atmospheric concentration of N_2O is determined by the natural balance between sources from land and ocean and the destruction of N_2O in the atmosphere largely by reaction with OH radicals (Crutzen, 1970; Johnston, 1971). The natural sources from land and ocean amount to ~ 6.6 and $3.8\,Tg\,N\,yr^{-1}$, respectively (Ciais et al., 2013). Anthropogenic activities currently add an additional $6.7\,Tg\,N\,yr^{-1}$ to the atmosphere that caused atmospheric N_2O to increase by 18 % since pre-industrial times (Ciais et al., 2013), reaching 325 ppb in the year 2012 (NOAA ESRL Global Monitoring Division, Boulder, Colorado, USA, http://esrl.noaa.gov/gmd/).

Using a compilation of 60 000 surface ocean observations of the partial pressure of N_2O (pN_2O), Nevison et al. (1995) computed a global ocean source of $4\,Tg\,N\,yr^{-1}$, with a large range of uncertainty from 1.2 to $6.8\,Tg\,N\,yr^{-1}$. Model derived estimates also differ widely, i.e., between 1.7 and $8\,Tg\,N\,yr^{-1}$ (Nevison et al., 2003; Suntharalingam et al., 2000). These large uncertainties are a consequence of too few observations and of poorly known N_2O formation mechanisms, reflecting a general lack of understanding of key elements of the oceanic nitrogen cycle (Gruber and Galloway, 2008; Zehr and Ward, 2002), and of N_2O in particular (e.g., Zamora et al., 2012; Bange et al., 2009; Freing et al., 2012, among others). A limited number of interior ocean N_2O observations were made available only recently (Bange et al., 2009), but they contain large temporal and spatial gaps. Information on the rates of many important processes remains insufficient, particularly in natural settings. There are only few studies from a limited number of specific regions such as the Arabian Sea, Central and North Pacific, the Bedford

BGD
11, 16703–16742, 2014

Basin and the Scheldt estuary, which can be used to derive and test model parameterizations (Mantoura et al., 1993; Bange et al., 2000; Elkins et al., 1978; Yoshida et al., 1989; Punshon and Moore, 2004; De Wilde and De Bie, 2000).

N_2O is formed in the ocean interior through two major pathways and consumed only in oxygen minimum zones through denitrification (Zamora et al., 2012). The first production pathway is associated with nitrification (conversion of ammonia, NH_4^+, into nitrate, NO_3^-), and occurs when dissolved O_2 concentrations are above 20 µmol L^{-1}. We subsequently refer to this pathway as the high-O_2 pathway. The second production pathway is associated with a series of processes when O_2 concentrations fall below ~ 5 µmol L^{-1} and involve a combination of nitrification and denitrification (hereinafter referred to as low-O_2 pathway) (Cohen and Gordon, 1978; Goreau et al., 1980; Elkins et al., 1978). As nitrification is one of the processes involved in the aerobic remineralization of organic matter, it occurs nearly everywhere in the global ocean with a global rate at least one order of magnitude larger than the global rate of water column denitrification (Gruber, 2008). A main reason is that denitrification in the water column is limited to the OMZs, which occupy only a few percent of the total ocean volume (Bianchi et al., 2012). This is also the only place in the water column where N_2O is being consumed.

The two production pathways have very different N_2O yields, i.e., fractions of nitrogen-bearing products that are transformed to N_2O. For the high-O_2 pathway, the yield is typically rather low, i.e., only about 1 in several hundred molecules of ammonium escapes as N_2O (Cohen and Gordon, 1979). In contrast, in the low-O_2 pathway, and particularly during denitrification, this fraction may go up to as high as 1 : 1, i.e., that all nitrate is turned into N_2O (Tiedje, 1988). The relative contribution of the two pathways to global N_2O production is not well established. Sarmiento and Gruber (2006) suggested that the two may be of equal importance, but more recent estimates suggest that the high-O_2 production pathway dominates global oceanic N_2O production (Freing et al., 2012).

Two strategies have been pursued in the development of parameterizations for N_2O production in global biogeochemical models. The first approach builds on the impor-

BGD
11, 16703–16742, 2014

tance of the nitrification pathway and its close association with the aerobic remineralization of organic matter. As a result the production of N_2O and the consumption of O_2 are closely tied to each other, leading to a strong correlation between the concentration of N_2O and the apparent oxygen utilization (AOU). This has led to the development of two sets of parameterizations, one based on concentrations, i.e., directly as a function of AOU (Butler et al., 1989) and the other based on the rate of oxygen utilization, i.e. OUR (Freing et al., 2009). Additional variables have been introduced to allow for differences in the yield, i.e., the ratio of N_2O produced over oxygen consumed, such as temperature (Butler et al., 1989) or depth (Freing et al., 2009). In the second approach, the formation of N_2O is modeled more mechanistically, and tied to both nitrification and denitrification by an O_2 dependent yield (Suntharalingam and Sarmiento, 2000; Nevison et al., 2003; Jin and Gruber, 2003). Since most models do not include nitrification explicitly, the formation rate is actually coupled directly to the remineralization of organic matter. Regardless of the employed strategy, all parameterizations depend to first order on the amount of organic matter that is being remineralized in the ocean interior, which is governed by the export of organic carbon to depth. The dependence of N_2O production on oxygen levels and on other parameters such as temperature only acts at second order. This has important implications not only for the modeling of the present-day distribution of N_2O in the ocean, but also for the sensitivity of marine N_2O to future climate change.

Over this century, climate change will perturb marine N_2O formation in multiple ways. Changes in productivity will drive changes in the export of organic matter to the ocean interior (Steinacher et al., 2010; Bopp et al., 2013) and hence affect the level of marine nitrification. Ocean warming might increase the rate of N_2O production during nitrification. Changes in carbonate chemistry (Bindoff et al., 2007) might cause changes in the C : N ratio of the exported organic matter (Riebesell et al., 2007), altering not only the rates of nitrification, but also the ocean interior oxygen levels (Gehlen et al., 2011). Finally, the expected general loss of oxygen (Keeling et al., 2010; Cocco et al., 2012; Bopp et al., 2013) could substantially affect denitrification and the N_2O production.

BGD
11, 16703–16742, 2014

Models used for IPCC's 4th assessment report estimated a decrease between 2 and 13 % in primary production (PP) under the business-as-usual high CO_2 concentration scenario A2 (Steinacher et al., 2010). A more recent multi-model analysis based on the models used in IPCC's 5th assessment report also suggest a large reduction of PP down to 18 % by 2100 for the RCP8.5 scenario (Bopp et al., 2013). In these simulations, the export of organic matter is projected to decrease between 6 and 18 % in 2100 (Bopp et al., 2013), with a spatially distinct pattern: in general, productivity and export are projected to decrease at mid- to low-latitudes in all basins, while productivity and export are projected to increase in the high-latitudes and in the South Pacific subtropical gyre (Bopp et al., 2013). A wider spectrum of responses was reported regarding changes in the ocean oxygen content. While all models simulate decreased oxygen concentrations in response to anthropogenic climate change (by about 2 to 4 % in 2100), and particularly in the mid-latitude thermocline regions, no agreement exists with regard to the hypoxic regions, i.e., those having oxygen levels below 60 $\mu mol\,L^{-1}$ (Cocco et al., 2012; Bopp et al., 2013). Some models project these regions to expand, while others project a contraction. Even more divergence in the results exists for the suboxic regions, i.e., those having O_2 concentrations below 5 $\mu mol\,L^{-1}$ (Keeling et al., 2010; Deutsch et al., 2011; Cocco et al., 2012; Bopp et al., 2013), although the trend for most models is pointing towards an expansion. At the same time, practically none of the models is able to correctly simulate the current distribution of oxygen in the OMZ (Bopp et al., 2013). In summary, while it is clear that major changes in ocean biogeochemistry are looming ahead (Gruber, 2011), with substantial impacts on the production and emission of N_2O, our ability to project these changes with confidence is limited.

In this study, we explore the implications of these future changes in ocean physics and biogeochemistry on the marine N_2O cycle, and make projections of the oceanic N_2O emissions from year 2005 to 2100 under the high CO_2 concentration scenario RCP8.5. We analyze how changes in biogeochemical and physical processes such as net primary production (NPP), export production and vertical stratification in this cen-

BGD
11, 16703–16742, 2014

tury translate into changes in oceanic N_2O emissions to the atmosphere. To this end, we use the NEMO-PISCES ocean biogeochemical model, which we have augmented with two different N_2O parameterizations, permitting us to evaluate changes in the marine N_2O cycle at the process level, especially with regard to production pathways in high and low oxygen regimes. We demonstrate that while future changes in the marine N_2O cycle will be substantial, the net emissions of N_2O appear to change relatively little, i.e., they are projected to decrease by about 10 % in 2100.

2 Methodology

2.1 NEMO-PISCES model

Future projections of the changes in the oceanic N_2O cycle were performed using the PISCES ocean biogeochemical model (Aumont and Bopp, 2006) in offline mode with physical forcings derived from the IPSL-CM5A-LR coupled model (Dufresne et al., 2013). The horizontal resolution of NEMO ocean general circulation model is $2^\circ \times 2^\circ \cos Ø$ (Ø being the latitude) with enhanced latitudinal resolution at the equator of 0.5°. PISCES is a biogeochemical model with five nutrients (NO_3, NH_4, PO_4, Si and Fe), two phytoplankton groups (diatoms and nanophytoplankton), two zooplankton groups (micro and mesozooplankton), and two non-living compartments (particulate and dissolved organic matter). Phytoplankton growth is limited by nutrient availability and light. Constant Redfield C : N : P ratios of 122 : 16 : 1 are assumed (Takahashi et al., 1985), while all other ratios, i.e., those associated with chlorophyll, iron, and silicon (Chl : C, Fe : C and Si : C) vary dynamically.

2.2 N_2O parameterizations in PISCES

We implemented two different parameterizations of N_2O production in NEMO-PISCES. The first one, adapted from Butler et al. (1989) follows the oxygen consumption approach, with a temperature dependent modification of the N_2O yield (P.TEMP). The

BGD
11, 16703–16742, 2014

second one is based on Jin and Gruber (2003) (P.OMZ), following the more mechanistic approach, i.e., it considers the different processes occurring at differing oxygen concentrations in a more explicit manner.

The P.TEMP parameterization assumes that the N_2O production is tied to nitrification only with a yield that is at first order constant. This is implemented in the model by tying the N_2O formation in a linear manner to O_2 consumption. A small temperature dependence is added to the yield to reflect the potential impact of temperature on metabolic rates. The production term of N_2O, i.e., $J^{\mathrm{P.TEMP}}(N_2O)$, is then mathematically formulated as:

$$J^{\mathrm{P.TEMP}}(N_2O) = (\gamma + \theta T) J(O_2)_{\mathrm{consumption}} \quad (1)$$

where γ is a background yield (0.53×10^{-4} mol N_2O (mol O_2 consumed)$^{-1}$), θ is the temperature dependency of γ (4.6×10^{-6} mol N_2O (mol O_2)$^{-1}$ K^{-1}), T is temperature (K), and $J(O_2)_{\mathrm{consumption}}$ is the sum of all biological O_2 consumption terms within the model. Although this parameterization is very simple, a recent analysis of N_2O observations supports such an essentially constant yield, even in the OMZ of the Eastern Tropical Pacific (Zamora et al., 2012).

The P.OMZ parameterization, formulated after Jin and Gruber (2003), assumes that the overall yield consists of a constant background yield and an oxygen dependent yield. The former is presumed to represent the N_2O production by nitrification, while the latter is presumed to reflect the enhanced production of N_2O at low oxygen concentrations, in part driven by denitrification, but possibly including nitrification as well. This parameterization includes the consumption of N_2O in suboxic conditions. This gives:

$$J^{\mathrm{P.OMZ}}(N_2O) = (\alpha + \beta f(O_2)) J(O_2)_{\mathrm{consumption}} - k N_2O \quad (2)$$

where α is, as in Eq. (1), a background yield (0.9×10^{-4} mol N_2O (mol O_2 consumed)$^{-1}$), β is a yield parameter that scales the oxygen dependent function (6.2×10^{-4}), $f(O_2)$

BGD
11, 16703–16742, 2014

is a unitless oxygen-dependent step-like modulating function, as suggested by laboratory experiments (Goreau et al., 1980) (Fig. S1, Supplement), and k is the 1st order rate constant of N_2O consumption close to anoxia (zero otherwise). For k, we have adopted a value of 0.138 yr^{-1} following Bianchi et al. (2012) while we set the consumption regime for O_2 concentrations below 5 $\mu mol\,L^{-1}$.

The P.OMZ parameterization permits us to separately identify the N_2O formation pathways associated with nitrification and those associated with low-oxygen concentrations (nitrification/denitrification). Specifically, we consider the source term $\alpha J(O_2)_{consumption}$ as that associated with the nitrification pathway, while we associated the source term $\beta f(O_2) J(O_2)_{consumption}$ with the low-oxygen processes (Fig. S2, Supplement).

We employ a standard bulk approach for simulating the loss of N_2O to the atmosphere via gas exchange. We use the formulation of Wanninkhof et al. (1992) for estimating the gas transfer velocity, adjusting the Schmidt number for N_2O and using the solubility constants of N_2O given by Weiss and Price (1980). We assume a constant atmospheric N_2O concentration of 284 ppb in all simulations.

2.3 Experimental design

NEMO-PISCES was first spun up during 3000 years using constant pre-industrial dynamical forcings fields from IPSL-CM5A-LR (Dufresne et al., 2013) without activating the N_2O parameterizations. This spin-up phase was followed by a 150 yr long simulation, forced by the same dynamical fields now with N_2O production and N_2O sea-to-air flux embedded. The N_2O concentration at all grid points was prescribed initially to 20 $nmol\,L^{-1}$, which is consistent with the MEMENTO database average value of 18 $nmol\,L^{-1}$ below 1500 m (Bange et al., 2009). During the 150 yr spin-up, we diagnosed the total N_2O production and N_2O sea-to-air flux and adjusted the α, β, γ and θ parameters in order to achieve a total N_2O sea-to-air flux in the two parameterizations at equilibrium close to 3.85 $Tg\,N\,yr^{-1}$ (Ciais et al., 2013). In addition, the relative con-

BGD
11, 16703–16742, 2014

tribution of the high-O_2 pathway in the P.OMZ parameterization was set to 75 % of the total N_2O production. This assumption is based on growing evidence that nitrification is the dominant pathway of N_2O production on a global scale, based on estimations considering N_2O production along with water mass transport (Freing et al., 2012).

Projections in NEMO-PISCES of historical (from 1851 to 2005) and future (from 2005 to 2100) simulated periods were done using dynamical forcing fields from IPSL-CM5A-LR. These dynamical forcings were applied in an offline mode, i.e. monthly means of temperature, velocity, wind speed or radiative flux were used to force NEMO-PISCES. Future simulations used the business-as-usual high CO_2 concentration scenario (RCP8.5) until year 2100. Century scale model drifts for all the biogeochemical variables presented, including N_2O sea-to-air flux, production and inventory, were removed using an additional control simulation with IPSL-CM5A-LR pre-industrial dynamical forcing fields from year 1851 to 2100. Despite the fact that primary production and the export of organic matter to depth were stable in the control simulation, the air–sea N_2O emissions drifted (an increase of 5 to 12 % in 200 yr depending on the parameterization) due to the short spin-up phase (150 yr) and to the choice of the initial conditions for N_2O concentrations.

3 Present-day oceanic N_2O

3.1 Contemporary N_2O fluxes

The model simulated air–sea N_2O emissions show large spatial contrasts, with flux densities varying by one order of magnitude, but with relatively small differences between the two parameterizations (Fig. 1a and b). This is largely caused by our assumption that the dominant contribution (75 %) to the total N_2O production in the P.OMZ parameterization is the nitrification pathway, which is then not so different from the P.TEMP parameterization, where it is 100 %. As a result, the major part of N_2O is produced close to the subsurface via nitrification, contributing directly to imprint changes

BGD
11, 16703–16742, 2014

into the sea-to-air N_2O flux without a significant meridional transport (Suntharalingam and Sarmiento, 2000).

Elevated N_2O emission regions ($> 50\,mg\,N\,m^{-2}\,yr^{-1}$) are found in the Eastern Tropical Pacific, in the northern Indian ocean, in the northwestern Pacific, in the North Atlantic and in the Agulhas Current. In contrast, low fluxes ($< 10\,mg\,N\,m^{-2}\,yr^{-1}$) are simulated in the Atlantic and Pacific subtropical gyres and southern Indian Ocean.

The regions of high N_2O emissions are in both parameterizations generally consistent with the data product of Nevison et al. (1995) (Fig. 1c), especially in the equatorial latitudes. The largest discrepancies occur in the North Pacific and Southern Ocean. The high N_2O emissions observed in the North Pacific are not well represented by our model, with a significant shift towards the western part of the Pacific basin, similar to other modeling studies (e.g., Goldstein et al., 2003; Jin and Gruber, 2003). The OMZ, located at approximately 600 m deep in the North Pacific, might be underestimated in our model, which in turn might suppress one potential N_2O source. Minor discrepancies between model and observations also occur in the Southern Ocean, a region whose role in global N_2O fluxes remains debated due to the lack of observations and the occurrence of potential artifacts due to interpolation techniques (e.g., Suntharalingam and Sarmiento, 2000; Nevison et al., 2003). In particular, the modeled N_2O flux maxima peak at around 40° S, i.e., around 10° N to that estimated by Nevison et al. (1995) (Fig. 1d).

3.2 Contemporary N_2O concentrations and the relationship to O_2

The model results at present day were evaluated against the MEMENTO database (Bange et al., 2009), which contains about 25 000 measurements of co-located N_2O and dissolved O_2 concentrations. Table 1 summarizes the SD and correlation coefficients for P.TEMP and P.OMZ compared to MEMENTO. The SD of the model output is very similar to MEMENTO, i.e., around 16 $nmol\,L^{-1}$ of N_2O. However, the correlation coefficients between the sampled data points from MEMENTO and P.TEMP/P.OMZ are 0.49 and 0.42, respectively.

BGD
11, 16703–16742, 2014

Figure 2 compares the global average vertical profile of the observed N_2O against the results from the two parameterisations. The in-situ observations show three characteristic layers: the upper 100 m layer with low ($\sim 10\,nmol\,L^{-1}$) N_2O concentration due to gas exchange keeping N_2O close to its saturation concentration, the mesopelagic layer, between 100 and 1500 m, where N_2O is enriched via nitrification and denitrification in the OMZs, and the deep ocean beyond 1500 m, with a relatively constant concentration of $18\,nmol\,L^{-1}$ on average. Both parameterizations underestimate the N_2O concentration in the upper 100 m, where most of the N_2O is potentially outgassed to the atmosphere. In the second layer, P.OMZ shows a good correlation with the observations, whereas P.TEMP is too low by $\sim 10\,nmol\,L^{-1}$. Below 1500 m, both parameterizations simulate too high N_2O compared to the observations. This may be caused by the lack or underestimation of a sink process in the deep ocean, or by the too high concentrations used to intialize the model, which persist due to the rather short spin-up time of only 150 yr.

The analysis of the model simulated N_2O concentrations as a function of model simulated O_2 shows the differences between the two parameterizations more clearly (Fig. 3a and b). Such a plot allows us to assess the model performance with regard to N_2O (Jin and Gruber, 2003), without being subject to the strong potential biases introduced by the model's deficiencies in simulating the distribution of O_2. This is particularly critical in the OMZs, where all models exhibit strong biases (Cocco et al., 2012; Bopp et al., 2013) (see also Fig. 3c). P.TEMP (Fig. 3a) slightly overestimates N_2O for dissolved O_2 concentrations above $100\,\mu mol\,L^{-1}$, and does not fully reproduce neither the high N_2O values in the OMZs nor the N_2O depletion when O_2 is almost completely consumed. P.OMZ (Fig. 3b) overestimates the N_2O concentration over the whole range of O_2, with particularly high values of N_2O above $100\,nmol\,L^{-1}$ due to the exponential function used in the OMZs. There, the observations suggest concentrations below $80\,nmol\,L^{-1}$ for the same low O_2 values, consistent with the linear trend observed for higher O_2, which seems to govern over most of the O_2 spectrum, as suggested by Zamora et al. (2012). The discrepancy at low O_2 concentration may also stem from

BGD
11, 16703–16742, 2014

our choice of a too low N_2O consumption rate under essentially anoxic conditions. The O_2 distribution in the model (Fig. 3c) shows a deficient representation of the OMZs, with higher concentrations than those from observations in the oxygen-corrected World Ocean Atlas (Bianchi et al., 2012). The rest of the O_2 spectrum is well represented in our model. Finally, it should be considered that most of the MEMENTO data points are from OMZs and therefore N_2O measurements could be biased towards higher values than the actual open ocean average, where our model performs better.

4 Future oceanic N_2O

4.1 N_2O sea-to-air flux

The global oceanic N_2O emissions decrease relatively little over the next century (Fig. 4a) between 4 and 12 %. Namely, in P.TEMP, the emissions decrease by 0.15 from 3.71 $Tg\,N\,yr^{-1}$ in 1985–2005 to 3.56 $Tg\,N\,yr^{-1}$ in 2080–2100 and in P.OMZ, the decrease is slightly larger at 12 % i.e., amounting to 0.49 $Tg\,N\,yr^{-1}$ from 4.03 to 3.54 $Tg\,N\,yr^{-1}$. Notable is also the presence of a negative trend in N_2O emissions over the 20th century, most pronounced in the P.OMZ parameterization. Considering the change over the 20th and 21st centuries together, the decreases increase to 7 and 15 %.

These relatively small global decreases mask more substantial changes at the regional scale, with a mosaic of regions experiencing a substantial increase and regions experiencing a substantial decrease (Fig. 4b and c). In both parameterizations, the oceanic N_2O emissions decrease in the northern and south western oceanic basins (e.g., the North Atlantic and Arabian Sea), by up to 25 $mg\,N\,m^{-2}\,yr^{-1}$. In contrast, the fluxes are simulated to increase in the Eastern Tropical Pacific and in the Bay of Bengal. For the Benguela Upwelling System (BUS) and the North Atlantic a bi-modal pattern emerges in 2100. As was the case for the present-day distribution of the N_2O fluxes,

BGD
11, 16703–16742, 2014

the overall similarity between the two parameterizations is a consequence of the dominance of the nitrification (high-O_2) pathway in both parameterizations.

Nevertheless there are two regions where more substantial differences between the two parameterizations emerge: the region overlying the oceanic OMZ at the BUS and the Southern Ocean. In particular, the P.TEMP parameterization projects a larger enhancement of the flux than P.OMZ at the BUS, whereas the emissions in the Southern Ocean are enhanced in the P.OMZ parameterization.

4.2 Drivers of changes in N_2O emissions

The changes in N_2O emissions may stem from a change in net N_2O production, a change in the transport of N_2O from its location of production to the surface, or any combination of the two, which includes also changes in N_2O storage. Next we determine the contribution of these mechanisms to the overall decrease in N_2O emissions that our model simulated for the 21st century.

4.2.1 Changes in N_2O production

In both parameterizations, global N_2O production is simulated to decrease over the 21st century. The total N_2O production in P.OMZ decreases by 0.41 $Tg\,N\,yr^{-1}$ in 2080–2100 compared to the mean value over 1985–2005 (Fig. 5a). The parameterization P.OMZ allows to isolate the contributions of high- and low-O_2 and will be analysed in greater detail in the following sections. N_2O production via the high-O_2 pathway in P.OMZ decreases in the same order than total production, by 0.35 $Tg\,N\,yr^{-1}$ in 2080–2100 compared to present. The N_2O production in the low-O_2 regions remains almost constant across the experiment. In P.TEMP parameterization, the reduction in N_2O production is much weaker than in P.OMZ due to the effect of the increasing temperature. N_2O production decreases by 0.07 $Tg\,N\,yr^{-1}$ in 2080–2100 compared to present (Fig. 5b).

BGD
11, 16703–16742, 2014

The vast majority of the changes in the N_2O production in the P.OMZ parameterization is caused by the high-O_2 pathway with virtually no contribution from the low-O_2 pathway (Fig. 5a). As the N_2O production in this pathway is solely driven by changes in the O_2 consumption (Eq. 2), which in our model is directly linked to export production, the dominance of this pathway implies that primary driver for the future changes in N_2O production in our model is the decrease in export of organic matter (CEX). It was simulated to decrease by $0.97\,Pg\,C\,yr^{-1}$ in 2100, and the high degree of correspondence in the temporal evolution of export and N_2O production in Fig. 5a confirms this conclusion.

The close connection between N_2O production associated with the high-O_2 pathway and changes in export production is also seen spatially (Fig. 5c), where the spatial pattern of changes in export and changes in N_2O production are extremely highly correlated (shown by stippling). Most of the small deviations are caused by lateral advection of organic carbon, causing a spatial separation between changes in O_2 consumption and changes in organic matter export.

As there is an almost ubiquitous decrease of export in all of the major oceanic basins except at high latitudes, N_2O production decreases overall as well. Hotspots of reductions exceeding $-10\,mg\,N\,m^{-2}\,yr^{-1}$ are found in the North Atlantic, the western Pacific and Indian basins (Fig. 5c). The fewer places where export increases, are also the locations of enhanced N_2O production. For example, a moderate increase of $3\,mg\,N\,m^{-2}\,yr^{-1}$ is projected in the Southern Ocean, South Atlantic and Eastern Tropical Pacific. The general pattern of export changes, i.e., decreases in lower latitudes, increase in higher latitudes, is consistent generally with other model projection patterns (Bopp et al., 2013), although there exist very strong model-to-model differences at the more regional scale.

Although the global contribution of the changes in the low-O_2 N_2O production is small, this is the result of regionally compensating trends. In the model's OMZs, i.e., in the Eastern Tropical Pacific and in the Bay of Bengal, a significant increase in N_2O production is simulated in these locations (Fig. 5d), with an increase of more than

BGD
11, 16703–16742, 2014

15 mg N m^{-2} yr^{-1}. This increase is primarily driven by the expansion of the OMZs in our model (shown by stippling), while changes in export contribute less. In effect, NEMO-PISCES projects a 20 % increase in the hypoxic volume globally, from 10.2 to 12.3 × 10^6 km^3, and an increase in the suboxic volume from 1.1 to 1.6 × 10^6 km^3 in 2100 (Fig. 5e). Elsewhere, the changes in the N_2O production through the low-O_2 pathway are dominated by the changes in export, thus following the pattern of the changes seen in the high-O_2 pathway. Overall these changes are negative, and happen to nearly completely compensate the increase in production in the OMZs, resulting in the near constant global N_2O production by the low-O_2 production pathway up to year 2100.

4.2.2 Changes in storage of N_2O

A steady increase in the N_2O inventory is observed from present to 2100. The pool of oceanic N_2O down to 1500 m, i.e., potentially outgassed to the atmosphere, increases by 8.9 Tg N from 1985–2005 to year 2100 in P.OMZ, whereas P.TEMP is less sensitive to changes with an increase of 4.0 Tg N on the time period considered (Fig. 6a).

This increase in storage of N_2O in the ocean interior shows an homogeneous pattern for P.TEMP, with particular hotspots in the North Pacific, North Atlantic and the eastern boundary currents in the Pacific (Fig. 6b). The spatial variability is more pronounced in P.OMZ (Fig. 6c), related in part to the enhanced production associated with OMZs. Most of the projected changes in storage are associated with shoaling of the mixed layer depth (shown by stippling), suggesting that increase in N_2O inventories is caused by increased ocean stratification. Enhanced ocean stratification, in turn, occurs in response to increasing sea surface temperatures associated with global warming (Sarmiento et al., 2004).

4.2.3 Effects of the combined mechanisms on N_2O emissions

The drivers of the future evolution of oceanic N_2O emissions emerge from the preceding analysis. Firstly, a decrease in the high-O_2 production pathway driven by a reduced

BGD
11, 16703–16742, 2014

organic matter remineralization reduces N_2O concentrations below the euphotic zone. Secondly, the increased N_2O inventory at depth is caused by increased stratification and therefore to a less efficient transport to the sea-to-air interface, leading to a less N_2O flux.

The global changes in N_2O flux, N_2O production and N_2O storage for P.OMZ are presented in Fig. 7. Changes in N_2O flux and N_2O production are mostly of the same sign in almost all of the oceanic regions in line with the assumption of nitrification being the dominant contribution to N_2O production. Changes in N_2O production close to the subsurface are translated into corresponding changes in N_2O flux. There is only one oceanic region (Sub-Polar Pacific) where this correlation does not occur. N_2O inventory increases in all of the oceanic regions. The increase in inventory is particularly pronounced at low latitudes along the eastern boundary currents in the Equatorial and Tropical Pacific. Figure 7 shows how almost all the relevant changes in N_2O production and storage are related to low-latitude processes, with little or no contribution from changes in polar regions.

The synergy among the driving mechanisms can be explored with a box model pursuing two objectives. First, to reproduce future projections assuming that the only mechanisms ruling the N_2O dynamics in the future were those that we have proposed in our hypothesis, i.e., increased stratification and reduction of N_2O production in high-O_2 regions. Secondly, to explore a wider range of values for both mixing (i.e., degree of stratification) and efficiency of N_2O production in high-O_2 conditions.

To this end, a box model was designed to explore the response of oceanic N_2O emissions to changes in export of organic matter (hence N_2O production only in high-O_2 conditions) and changes in the mixing ratio between deep (> 100 m) and surface (< 100 m) layers. We divided the water column into two compartments: a surface layer in the upper 100 m where 80 % of surface N_2O concentration is outgassed to the atmosphere (Eq. 3), and a deeper layer beyond 100 m, where N_2O is produced from remineralization as a fraction of the organic matter exported in the ocean interior (Eq. 4). The N_2O reservoirs in the surface and in the deep layer are allowed to exchange. The

BGD
11, 16703–16742, 2014

exchange is regulated by a mixing coefficient ν:

$$\text{surface } N_2O; \quad \frac{dN_2O^s}{dt} = -\nu \cdot \left(N_2O^s - N_2O^d\right) - \kappa \cdot N_2O^s \tag{3}$$

$$\text{deep } N_2O; \quad \frac{dN_2O^d}{dt} = \nu \cdot \left(N_2O^s - N_2O^d\right) + \varepsilon \cdot \Phi^{POC} \tag{4}$$

where N_2O^s is N_2O in the surface, N_2O^d is N_2O in the deep reservoir, Φ^{POC} is the flux of POC into the lower compartment, ν is the mixing coefficient between both compartments, k is the fraction of N_2O^s outgassed to the atmosphere and ε the fraction of POC leading to N_2O^d formation (Fig. S3 and Table S1, Supplement). Equations (3) and (4) are solved for a combination of POC fluxes and mixing coefficients, reflecting the increasing stratification and the decrease in export production projected by year 2100 (Sarmiento et al., 2004; Bopp et al., 2013).

A decrease in the N_2O flux is observed for a wide range of boundary conditions simulating reduced mixing and export of POC (Fig. 8a). The equivalent of the transient NEMO-PISCES simulation, i.e., a −10 % decrease in N_2O flux, is achieved for a −8 % decrease in export in the box model. The most extreme scenario explored with the box model suggests a −20 % decrease in N_2O flux, although these associated values of mixing and export are clearly unrealistic, from a nearly total stagnation of ocean circulation between the deep and surface layers to an attenuation of export of −20 % in the global ocean.

The projected increase in N_2O storage in the deep reservoir is reproduced by the box model (Fig. 8b) at a wide range of changes particularly in mixing. Changes in mixing dominate over changes in export as drivers of the increase in the N_2O reservoir at depth. A 25 % decrease in mixing leads to an increase in storage similar to the one projected with NEMO-PISCES (+10 %), independently of changes in export of organic matter.

In general, the interplay between mixing and export of organic matter operates differently when N_2O flux or N_2O inventory are considered. The box model experiment

BGD
11, 16703–16742, 2014

suggests that the evolution of the N_2O reservoir is driven almost entirely by changes in mixing, while changes of mixing and export of organic matter have similar relevance when modulating N_2O emissions.

5 Caveats in estimating N_2O using ocean biogeochemical models

The use of O_2 consumption as a proxy for the actual N_2O production expand the uncertainties in N_2O model estimations. Future model development should aim at the implementation of mechanistic parameterizations of N_2O production based on nitrification and denitrification rates. Further, in order to determine accurate O_2 boundaries for both N_2O production and N_2O consumption at the core of OMZs additional measurements and microbial experiments are needed. The contribution of the high-O_2 pathway that was considered in this model analysis might be a conservative estimate. Freing et al. (2012) suggested that the high-O_2 pathway could be responsible of 93 % of the total N_2O production. Assuming that changes in the N_2O flux are mostly driven by N_2O production via nitrification, that would suggest a larger reduction in the marine N_2O emissions in the future. Moreover, Zamora et al. (2012) observed a higher than expected N_2O consumption at the core of the OMZ in the Eastern Tropical Pacific, occurring at an upper threshold of 10 µmol L^{-1}. The contribution of OMZs to total N_2O production remains an open question. N_2O formation associated with OMZs might be counterbalanced by its own local consumption, leading to the attenuation of the only increasing source of N_2O attributable to the projected future expansion of OMZs (Steinacher et al., 2010; Bopp et al., 2013). Finally, the accurate representation of subsurface O_2 concentration remains as a major challenge for ocean biogeochemical models, as shown by Bopp et al. (2013).

The combined effect of climate change and ocean acidification has not been analyzed in this study. N_2O production processes might be altered by the response of nitrification to increasing levels of seawater pCO_2 (Huesemann et al., 2002; Beman et al., 2011). Beman et al. (2011) reported a reduction in nitrification in response to

BGD
11, 16703–16742, 2014

decreasing pH. This result suggests that N_2O production might decrease beyond what we have estimated only due to climate change. Conversely, negative changes in the ballast effect could potentially reinforce nitrification at shallow depth in response to less efficient POC export to depth and shallow remineralization (Gehlen et al., 2011). Regarding N_2O formation via denitrification, changes in seawater pH as a consequence of higher levels of CO_2 might not be substantial enough to change the N_2O production efficiency, assuming a similar response of marine denitrifiers as reported for denitrifying bacteria have in terrestrial systems (Liu et al., 2010). Finally, the C : N ratio in export production (Riebesell et al., 2007) might increase in response to ocean acidification, potentially leading to a greater expansion of OMZs than simulated here (Oschlies et al., 2008; Tagliabue et al., 2011), and therefore to enhanced N_2O production associated with the low-O_2 pathway.

Changes in atmospheric nitrogen deposition have not been considered in this study. It has been suggested that due to anthropogenic activities the additional amount of reactive nitrogen in the ocean could fuel primary productivity and N_2O production. Estimates are however low, around 3–4 % of the total oceanic emissions (Suntharalingam et al., 2012).

Longer simulation periods could reveal additional effects on N_2O transport beyond changes in upwelling or meridional transport of N_2O close to the subsurface (Suntharalingam and Sarmiento, 2000). Eventual ventilation of the N_2O reservoir at high latitudes could shed light into the role of upwelling regions as an important source of N_2O. Additional studies using other ocean biogeochemical models might also yield alternative values using the same parameterizations. N_2O production is particularly sensitive to the distribution and magnitude of export of organic matter and O_2 fields defined in models.

BGD
11, 16703–16742, 2014

6 Contribution of future N_2O to climate feedbacks

Changes in the oceanic emissions of N_2O to the atmosphere will have an impact on atmospheric radiative forcing, with potential feedbacks on the climate system. Based on the estimated 4 to 12 % decrease in N_2O sea-to-air flux over the 21st century under RCP8.5, we estimated the feedback factor for these changes as defined by Xu-Ri et al. (2012). Considering the reference value of the pre-industrial atmospheric N_2O concentration of 280 ppb in equilibrium, and its associated global N_2O emissions of 11.8 $Tg\,N\,yr^{-1}$, we quantify the resulting changes in N_2O concentration per degree for the two projected emissions in 2100 using P.TEMP and P.OMZ. The model projects changes in N_2O emissions of −0.16 and −0.48 $Tg\,N\,yr^{-1}$ respectively, whereas surface temperature is assumed to increase globally by 3 °C on average according to the physical forcing used in our simulations. These results yield −0.05 and −0.16 $Tg\,N\,yr^{-1}\,K^{-1}$, or alternatively −1.25 and −3.8 $ppb\,K^{-1}$ for P.TEMP and P.OMZ respectively. Using Joos et al. (2001) we calculate the feedback factor in equilibrium for projected changes in emissions to be −0.005 and −0.014 $W\,m^{-2}\,K^{-1}$ in P.TEMP and P.OMZ.

Stocker et al. (2013) projected changes in terrestrial N_2O emissions in 2100 using transient model simulations leading to feedback strengths between +0.001 and +0.015 $W\,m^{-2}\,K^{-1}$. Feedback strengths associated with the projected decrease of oceanic N_2O emissions are of the same order of magnitude as those attributable to changes in the terrestrial sources of N_2O, yet opposite in sign, suggesting a compensation of changes in radiative forcing due to future increasing terrestrial N_2O emissions. At this stage, potential compensation between land and ocean emissions is to be taken with caution, as it relies of a single model run with constant atmospheric N_2O.

7 Conclusions

Our simulations suggest that anthropogenic climate change could lead to a global decrease in oceanic N_2O emissions during the 21st century. This maximum projected de-

BGD
11, 16703–16742, 2014

crease of 12 % in marine N_2O emissions for the business-as-usual high CO_2 emissions scenario would compensate for the estimated increase in N_2O fluxes from the terrestrial biosphere in response to anthropogenic climate change (Stocker et al., 2013), so that the climate–N_2O feedback may be more or less neutral over the coming decades.

The main mechanisms contributing to the reduction of marine N_2O emissions are a decrease in N_2O production in high oxygenated waters as well as an increase in ocean vertical stratification that acts to decrease the transport of N_2O from the subsurface to the surface ocean. Despite the decrease in both N_2O production and N_2O emissions, simulations suggest that the global marine N_2O inventory may increase from 2005 to 2100. This increase is explained by the reduced transport of N_2O from the production zones to the air–sea interface.

Differences between the two parameterizations used here are modest, and the role of warming in P.TEMP or higher N_2O yields at low-O_2 concentrations in P.OMZ does not translate into significant differences in our model projections. The dominant high-O_2 N_2O production pathway drives not only the general decrease in N_2O emissions but also the homogeneousness between the two parameterizations considered.

The N_2O production pathways demand however a better understanding in order to enable an improved representation of processes in models. At a first order, the efficiencies of the production processes in response to higher temperatures or increased seawater pCO_2 are required. Second order effects such as changes in the O_2 boundaries at which nitrification and denitrification occur must be also taken into account. In the absence of process-based parameterizations, N_2O production parameterizations will still rely on export of organic carbon and oxygen levels. Both need to be improved in global biogeochemical models.

The same combination of mechanisms (i.e., change in export production and ocean stratification) have been identified as drivers of changes in oceanic N_2O emissions during the Younger Dryas by Goldstein et al. (2003). The N_2O flux decreased, while the N_2O reservoir was fueled by longer residence times of N_2O caused by increased

BGD
11, 16703–16742, 2014

stratification. Whether these mechanisms are plausible drivers of changes beyond year 2100 remains an open question that needs to be addressed with longer simulations.

The Supplement related to this article is available online at doi:10.5194/bgd-11-16703-2014-supplement.

Acknowledgements. We thank Cynthia Nevison for providing us the N_2O sea-to-air flux dataset. We thank Annette Kock and Herman Bange for the availability of the MEMENTO database (https://memento.geomar.de). Comments by Parvadha Suntharalingam improved significantly this manuscript. Nicolas Gruber acknowledges the support of ETH Zürich. This work has been supported by the European Union via the Greencycles II FP7-PEOPLE-ITN-2008, number 238366. We thank Christian Ethé for help analyzing PISCES model drift.

References

Aumont, O. and Bopp, L.: Globalizing results from ocean in situ iron fertilization studies, Global Biogeochem. Cy., 20, GB2017, doi:10.1029/2005gb002591, 2006.

Bange, H. W., Rixen, T., Johansen, A. M., Siefert, R. L., Ramesh, R., Ittekkot, V., Hoffmann, M. R., and Andreae, M. O.: A revised nitrogen budget for the Arabian Sea, Global Biogeochem. Cy., 14, 1283–1297, doi:10.1029/1999gb001228, 2000.

Bange, H. W., Bell, T. G., Cornejo, M., Freing, A., Uher, G., Upstill-Goddard, R. C., and Zhang, G.: MEMENTO: a proposal to develop a database of marine nitrous oxide and methane measurements, Environ. Chem., 6, 195–197, doi:10.1071/en09033, 2009.

Beman, J. M., Chow, C.-E., King, A. L., Feng, Y., Fuhrman, J. A., Andersson, A., Bates, N. R., Popp, B. N., and Hutchins, D. A.: Global declines in oceanic nitrification rates as a consequence of ocean acidification, P. Natl. Acad. Sci. USA, 108, 208–213, doi:10.1073/pnas.1011053108, 2011.

Bianchi, D., Dunne, J. P., Sarmiento, J. L., and Galbraith, E. D.: Data-based estimates of suboxia, denitrification, and N_2O production in the ocean and their sensitivities to dissolved O_2, Global Biogeochem. Cy., 26, GB2009, doi:10.1029/2011gb004209, 2012.

BGD
11, 16703–16742, 2014

Bindoff, N., Willebrand, J., Artale, V., Cazenave, A., Gregory, J., Gulev, S., Hanawa, K., Le Quere, C., Levitus, S., Norjiri, Y., Shum, C., Talley, L., and Unnikrishnan, A.: Observations: oceanic climate change and sea level, in: Climate Change 2007: The Physical Science Basis. Contribution of Working Group I to the Fourth Assessment Report of the Intergovernmental Panel on Climate Change, 2007.

Bopp, L., Resplandy, L., Orr, J. C., Doney, S. C., Dunne, J. P., Gehlen, M., Halloran, P., Heinze, C., Ilyina, T., Séférian, R., Tjiputra, J., and Vichi, M.: Multiple stressors of ocean ecosystems in the 21st century: projections with CMIP5 models, Biogeosciences, 10, 6225–6245, doi:10.5194/bg-10-6225-2013, 2013.

Butler, J. H., Elkins, J. W., Thompson, T. M., and Egan, K. B.: Tropospheric and dissolved N_2O of the west pacific and east-indian oceans during the El-Niño Southern Oscillation event of 1987, J. Geophys. Res.-Atmos., 94, 14865–14877, doi:10.1029/JD094iD12p14865, 1989.

Ciais, P., Sabine, C., Bala, G., Bopp, L., Brovkin, V., Canadell, J., Chhabra, A., DeFries, R., Galloway, J., Heimann, M., Jones, C., Le Quéré, C., Myneni, R. B., Piao, S., and Thornton, P.: Carbon and other biogeochemical cycles, in: Climate Change 2013: The Physical Science Basis. Contribution of Working Group I to the Fifth Assessment Report of the Intergovernmental Panel on Climate Change, 2013.

Cocco, V., Joos, F., Steinacher, M., Frölicher, T. L., Bopp, L., Dunne, J., Gehlen, M., Heinze, C., Orr, J., Oschlies, A., Schneider, B., Segschneider, J., and Tjiputra, J.: Oxygen and indicators of stress for marine life in multi-model global warming projections, Biogeosciences, 10, 1849–1868, doi:10.5194/bg-10-1849-2013, 2013.

Cohen, Y. and Gordon, L. I.: Nitrous-oxide in oxygen minimum of eastern tropical north pacific – evidence for its consumption during denitrification and possible mechanisms for its production, Deep-Sea Res., 25, 509–524, doi:10.1016/0146-6291(78)90640-9, 1978.

Cohen, Y. and Gordon, L. I.: Nitrous-oxide production in the ocean, J. Geophys. Res.-Oceans, 84, 347–353, doi:10.1029/JC084iC01p00347, 1979.

Crutzen, P. J.: Influence of nitrogen oxides on atmospheric ozone content, Q. J. Roy. Meteor. Soc., 96, 320–326, doi:10.1002/qj.49709640815, 1970.

de Wilde, H. P. J. and de Bie, M. J. M.: Nitrous oxide in the Schelde estuary: production by nitrification and emission to the atmosphere, Mar. Chem., 69, 203–216, doi:10.1016/s0304-4203(99)00106-1, 2000.

Deutsch, C., Brix, H., Ito, T., Frenzel, H., and Thompson, L.: Climate-forced variability of ocean hypoxia, Science, 333, 336–339, doi:10.1126/science.1202422, 2011.

BGD
11, 16703–16742, 2014

Dufresne, J. L., Foujols, M. A., Denvil, S., Caubel, A., Marti, O., Aumont, O., Balkanski, Y., Bekki, S., Bellenger, H., Benshila, R., Bony, S., Bopp, L., Braconnot, P., Brockmann, P., Cadule, P., Cheruy, F., Codron, F., Cozic, A., Cugnet, D., de Noblet, N., Duvel, J. P., Ethe, C., Fairhead, L., Fichefet, T., Flavoni, S., Friedlingstein, P., Grandpeix, J. Y., Guez, L., Guilyardi, E., Hauglustaine, D., Hourdin, F., Idelkadi, A., Ghattas, J., Joussaume, S., Kageyama, M., Krinner, G., Labetoulle, S., Lahellec, A., Lefebvre, M. P., Lefevre, F., Levy, C., Li, Z. X., Lloyd, J., Lott, F., Madec, G., Mancip, M., Marchand, M., Masson, S., Meurdesoif, Y., Mignot, J., Musat, I., Parouty, S., Polcher, J., Rio, C., Schulz, M., Swingedouw, D., Szopa, S., Talandier, C., Terray, P., Viovy, N., and Vuichard, N.: Climate change projections using the IPSL-CM5 Earth System Model: from CMIP3 to CMIP5, Clim. Dynam., 40, 2123–2165, doi:10.1007/s00382-012-1636-1, 2013.

Elkins, J. W., Wofsy, S. C., McElroy, M. B., Kolb, C. E., and Kaplan, W. A.: Aquatic sources and sinks for nitrous-oxide, Nature, 275, 602–606, doi:10.1038/275602a0, 1978.

Freing, A., Wallace, D. W. R., Tanhua, T., Walter, S., and Bange, H. W.: North Atlantic production of nitrous oxide in the context of changing atmospheric levels, Global Biogeochem. Cy., 23, GB4015, doi:10.1029/2009gb003472, 2009.

Freing, A., Wallace, D. W. R., and Bange, H. W.: Global oceanic production of nitrous oxide, Philos. T. R. Soc. B, 367, 1245–1255, doi:10.1098/rstb.2011.0360, 2012.

Gehlen, M., Gruber, N., Gangstø, R., Bopp, L., and Oschlies, A.: Biogeochemical consequences of ocean acidification and feedbacks to the earth system, in: Ocean Acidification, 230–248, 2011.

Goldstein, B., Joos, F., and Stocker, T. F.: A modeling study of oceanic nitrous oxide during the Younger Dryas cold period, Geophys. Res. Lett., 30, 1092, doi:10.1029/2002gl016418, 2003.

Goreau, T. J., Kaplan, W. A., Wofsy, S. C., McElroy, M. B., Valois, F. W., and Watson, S. W.: Production of NO_2^- and N_2O by nitrifying bacteria at reduced concentrations of oxygen, Appl. Environ. Microb., 40, 526–532, 1980.

Gruber, N.: The marine nitrogen cycle: overview of distributions and processes, in: Nitrogen in the Marine Environment, 2nd edn., 1–50, 2008.

Gruber, N.: Warming up, turning sour, losing breath: ocean biogeochemistry under global change, Philos. T. R. Soc. A, 369, 1980–1996, doi:10.1098/rsta.2011.0003, 2011.

Gruber, N. and Galloway, J. N.: An Earth-system perspective of the global nitrogen cycle, Nature, 451, 293–296, doi:10.1038/nature06592, 2008.

BGD
11, 16703–16742, 2014

Huesemann, M. H., Skillman, A. D., and Crecelius, E. A.: The inhibition of marine nitrification by ocean disposal of carbon dioxide, Mar. Pollut. Bull., 44, 142–148, doi:10.1016/s0025-326x(01)00194-1, 2002.

Jin, X. and Gruber, N.: Offsetting the radiative benefit of ocean iron fertilization by enhancing N_2O emissions, Geophys. Res. Lett., 30, 2249, doi:10.1029/2003gl018458, 2003.

Johnston, H.: Reduction of stratospheric ozone by nitrogen oxide catalysts from supersonic transport exhaust, Science, 173, 517–522, doi:10.1126/science.173.3996.517, 1971.

Joos, F., Prentice, I. C., Sitch, S., Meyer, R., Hooss, G., Plattner, G. K., Gerber, S., and Hasselmann, K.: Global warming feedbacks on terrestrial carbon uptake under the Intergovernmental Panel on Climate Change (IPCC) emission scenarios, Global Biogeochem. Cy., 15, 891–907, doi:10.1029/2000gb001375, 2001.

Keeling, R. F., Koertzinger, A., and Gruber, N.: Ocean deoxygenation in a warming world, Ann. Rev. Mar. Sci., 2, 199–229, doi:10.1146/annurev.marine.010908.163855, 2010.

Liu, B., Morkved, P. T., Frostegard, A., and Bakken, L. R.: Denitrification gene pools, transcription and kinetics of NO, N_2O and N_2 production as affected by soil pH, FEMS Microbiol. Ecol., 72, 407–417, doi:10.1111/j.1574-6941.2010.00856.x, 2010.

Mantoura, R. F. C., Law, C. S., Owens, N. J. P., Burkill, P. H., Woodward, E. M. S., Howland, R. J. M., and Llewellyn, C. A.: Nitrogen biogeochemical cycling in the northwestern indian-ocean, Deep-Sea Res. Pt. II, 40, 651–671, 1993.

Myhre, G., Shindell, D., Bréon, F.-M., Collins, W., Fuglestvedt, J., Huang, J., Koch, D., Lamarque, J.-F., Lee, D., Mendoza, B., Nakajima, T., Robock, A., Stephens, G., Takemura, T., and Zhang, H.: Anthropogenic and natural radiative forcing, in: Climate Change 2013: The Physical Science Basis. Contribution of Working Group I to the Fifth Assessment Report of the Intergovernmental Panel on Climate Change, 2013.

Nevison, C., Butler, J. H., and Elkins, J. W.: Global distribution of N_2O and the Delta N_2O-AOU yield in the subsurface ocean, Global Biogeochem. Cy., 17, 1119, doi:10.1029/2003gb002068, 2003.

Nevison, C. D., Weiss, R. F., and Erickson, D. J.: Global oceanic emissions of nitrous-oxide, J. Geophys. Res.-Oceans, 100, 15809–15820, doi:10.1029/95jc00684, 1995.

Oschlies, A., Schulz, K. G., Riebesell, U., and Schmittner, A.: Simulated 21st century's increase in oceanic suboxia by CO_2-enhanced biotic carbon export, Global Biogeochem. Cy., 22, GB4008, doi:10.1029/2007gb003147, 2008.

BGD
11, 16703–16742, 2014

Prather, M. J., Holmes, C. D., and Hsu, J.: Reactive greenhouse gas scenarios: systematic exploration of uncertainties and the role of atmospheric chemistry, Geophys. Res. Lett., 39, L09803, doi:10.1029/2012gl051440, 2012.

Punshon, S. and Moore, R. M.: Nitrous oxide production and consumption in a eutrophic coastal embayment, Mar. Chem., 91, 37–51, doi:10.1016/j.marchem.2004.04.003, 2004.

Ravishankara, A. R., Daniel, J. S., and Portmann, R. W.: Nitrous oxide (N_2O): the dominant ozone-depleting substance emitted in the 21st century, Science, 326, 123–125, doi:10.1126/science.1176985, 2009.

Resplandy, L., Lévy, M., Bopp, L., Echevin, V., Pous, S., Sarma, V. V. S. S., and Kumar, D.: Controlling factors of the oxygen balance in the Arabian Sea's OMZ, Biogeosciences, 9, 5095–5109, doi:10.5194/bg-9-5095-2012, 2012.

Riebesell, U., Schulz, K. G., Bellerby, R. G. J., Botros, M., Fritsche, P., Meyerhoefer, M., Neill, C., Nondal, G., Oschlies, A., Wohlers, J., and Zoellner, E.: Enhanced biological carbon consumption in a high CO_2 ocean, Nature, 450, 545–548, doi:10.1038/nature06267, 2007.

Sarmiento, J. L., Slater, R., Barber, R., Bopp, L., Doney, S. C., Hirst, A. C., Kleypas, J., Matear, R., Mikolajewicz, U., Monfray, P., Soldatov, V., Spall, S. A., and Stouffer, R.: Response of ocean ecosystems to climate warming, Global Biogeochem. Cy., 18, GB3003, doi:10.1029/2003gb002134, 2004.

Steinacher, M., Joos, F., Frölicher, T. L., Bopp, L., Cadule, P., Cocco, V., Doney, S. C., Gehlen, M., Lindsay, K., Moore, J. K., Schneider, B., and Segschneider, J.: Projected 21st century decrease in marine productivity: a multi-model analysis, Biogeosciences, 7, 979–1005, doi:10.5194/bg-7-979-2010, 2010.

Stocker, B. D., Roth, R., Joos, F., Spahni, R., Steinacher, M., Zaehle, S., Bouwman, L., Xu, R., and Prentice, I. C.: Multiple greenhouse-gas feedbacks from the land biosphere under future climate change scenarios, Nat. Clim. Change, 3, 666–672, doi:10.1038/nclimate1864, 2013.

Suntharalingam, P. and Sarmiento, J. L.: Factors governing the oceanic nitrous oxide distribution: simulations with an ocean general circulation model, Global Biogeochem. Cy., 14, 429–454, doi:10.1029/1999gb900032, 2000.

Suntharalingam, P., Sarmiento, J. L., and Toggweiler, J. R.: Global significance of nitrous-oxide production and transport from oceanic low-oxygen zones: a modeling study, Global Biogeochem. Cy., 14, 1353–1370, doi:10.1029/1999gb900100, 2000.

Suntharalingam, P., Buitenhuis, E., Le Quere, C., Dentener, F., Nevison, C., Butler, J. H., Bange, H. W., and Forster, G.: Quantifying the impact of anthropogenic nitrogen deposi-

BGD
11, 16703–16742, 2014

tion on oceanic nitrous oxide, Geophys. Res. Lett., 39, L07605, doi:10.1029/2011gl050778, 2012.
Tagliabue, A., Bopp, L., and Gehlen, M.: The response of marine carbon and nutrient cycles to ocean acidification: large uncertainties related to phytoplankton physiological assumptions, Global Biogeochem. Cy., 25, GB3017, doi:10.1029/2010gb003929, 2011.
Takahashi, T., Broecker, W. S., and Langer, S.: Redfield ratio based on chemical-data from isopycnal surfaces, J. Geophys. Res.-Oceans, 90, 6907–6924, doi:10.1029/JC090iC04p06907, 1985.
Tiedje, J. M.: Ecology of denitrification and dissimilatory nitrate reduction to ammonium, in: Biology of Anaerobic Microorganisms, 179–244, 1988.
Wanninkhof, R.: Relationship between wind-speed and gas-exchange over the ocean, J. Geophys. Res.-Oceans, 97, 7373–7382, doi:10.1029/92jc00188, 1992.
Weiss, R. F. and Price, B. A.: Nitrous-oxide solubility in water and seawater, Mar. Chem., 8, 347–359, doi:10.1016/0304-4203(80)90024-9, 1980.
Yoshida, N., Morimoto, H., Hirano, M., Koike, I., Matsuo, S., Wada, E., Saino, T., and Hattori, A.: Nitrification rates and N-15 abundances of N_2O and NO_3^- in the western north pacific, Nature, 342, 895–897, doi:10.1038/342895a0, 1989.
Zamora, L. M., Oschlies, A., Bange, H. W., Huebert, K. B., Craig, J. D., Kock, A., and Löscher, C. R.: Nitrous oxide dynamics in low oxygen regions of the Pacific: insights from the MEMENTO database, Biogeosciences, 9, 5007–5022, doi:10.5194/bg-9-5007-2012, 2012.
Zehr, J. P. and Ward, B. B.: Nitrogen cycling in the ocean: new perspectives on processes and paradigms, Appl. Environ. Microb., 68, 1015–1024, doi:10.1128/aem.68.3.1015-1024.2002, 2002.

BGD
11, 16703–16742, 2014

Table 1. SD and correlation coefficients between P.TEMP and P.OMZ parameterizations with respect to MEMENTO database observations (Bange et al., 2009).

	P.TEMP	P.OMZ	OBS
SD (in nmol $N_2O\,L^{-1}$)	12	18	16
Correlation coefficient with obs.	0.49	0.42	–

BGD
11, 16703–16742, 2014

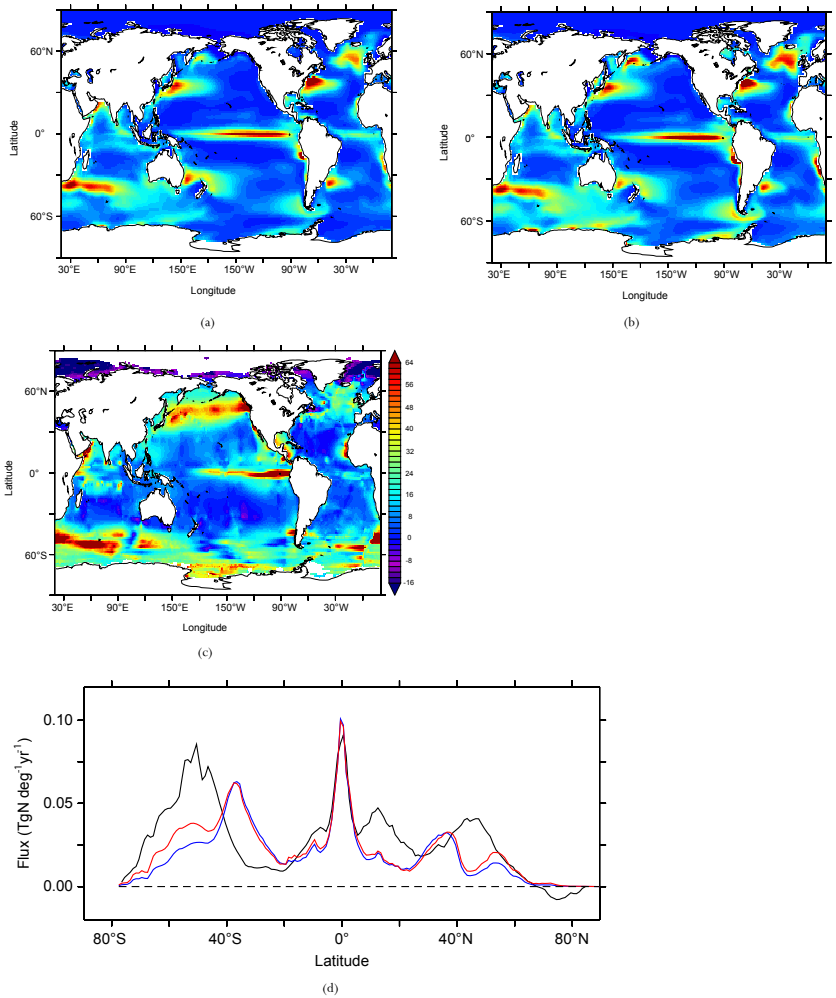

BGD
11, 16703–16742, 2014

Oceanic N_2O emissions in the 21st century

J. Martinez-Rey et al.

Figure 1. N_2O sea-to-air flux (in $mg\,N\,m^{-2}\,yr^{-1}$) from **(a)** P.TEMP parameterzation averaged for the 1985 to 2005 time period in the historical simulation, **(b)** P.OMZ parameterization over the same time period, **(c)** data product of Nevison et al. (1995) and **(d)** latitudinal N_2O sea-to-air flux (in $Tg\,N\,deg^{-1}\,yr^{-1}$) from Nevison et al. (1995) (black), P.TEMP (blue) and P.OMZ (red).

BGD
11, 16703–16742, 2014

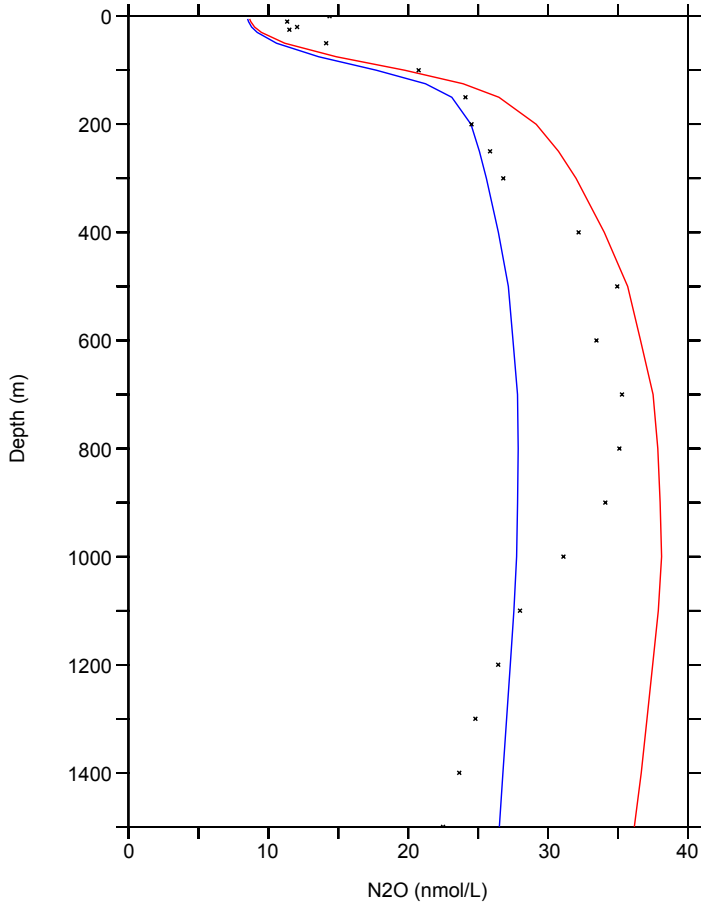

Figure 2. Global average depth profile of N_2O concentration (in nmol L^{-1}) from the MEMENTO database (dots) (Bange et al., 2009), P.TEMP (blue) and P.OMZ (red). Model parameterizations are averaged over the 1985 to 2005 time period from the historical simulation.

BGD
11, 16703–16742, 2014

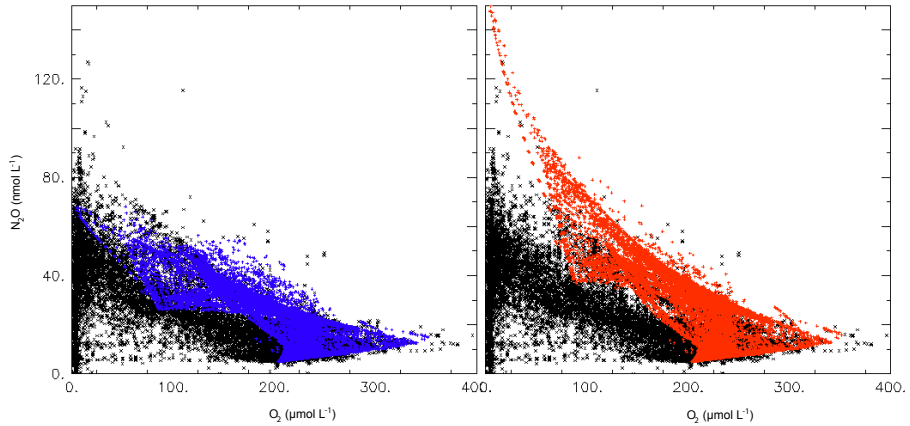

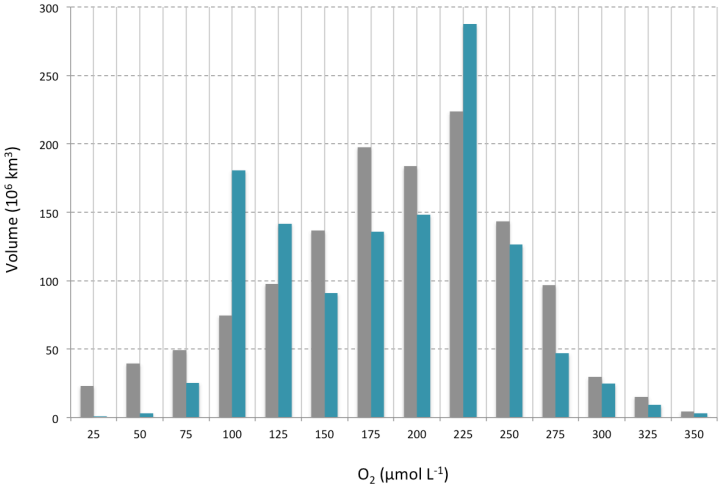

BGD
11, 16703–16742, 2014

Oceanic N_2O emissions in the 21st century

J. Martinez-Rey et al.

Figure 3. Relationship between O_2 concentration (in $\mu mol\,L^{-1}$) and N_2O concentration (in $nmol\,L^{-1}$) in the MEMENTO database (black) (Bange et al., 2009), compared to model **(a)** P.TEMP (blue) and **(b)** P.OMZ (red) parameterizations averaged over the 1985 to 2005 time period from the historical simulation. **(c)** Distribution of O_2 concentration in NEMO-PISCES 1985 to 2005 averaged time period (blue) compared to the oxygen corrected World Ocean Atlas (grey) from Bianchi et al. (2012).

BGD
11, 16703–16742, 2014

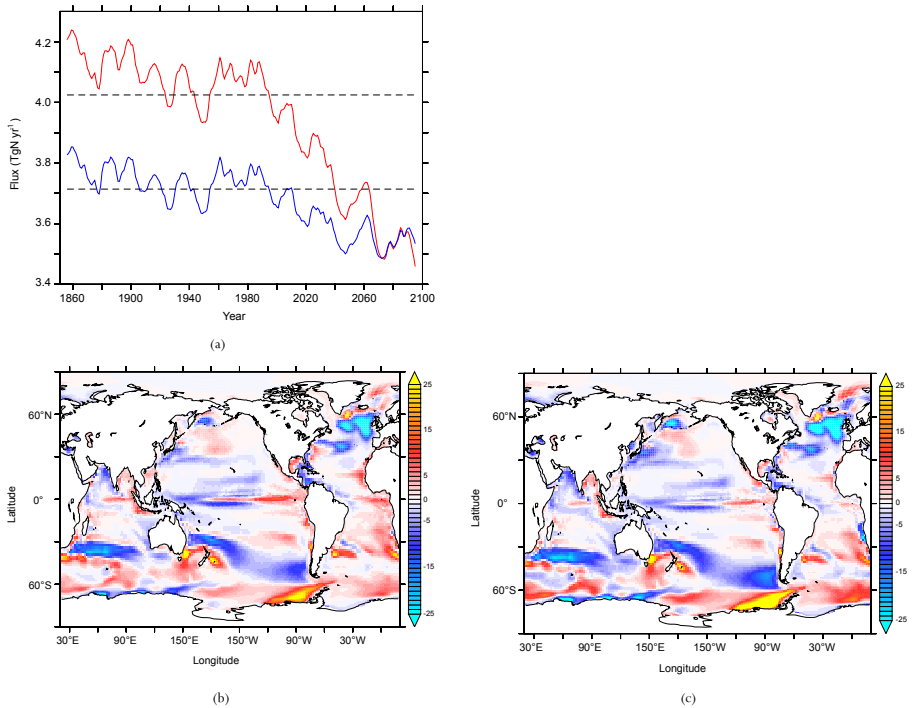

Figure 4. (a) N_2O sea-to-air flux (in $Tg\,N\,yr^{-1}$) from 1851 to 2100 in P.TEMP (blue) and P.OMZ (red) using the historical and future RCP8.5 simulations. Dashed lines indicate the mean value over the 1985 to 2005 time period. Change in N_2O sea-to-air flux ($mg\,N\,m^{-2}\,yr^{-1}$) from the averaged 2080–2100 to 1985–2005 time periods in future RCP8.5 and historical simulations in **(b)** P.TEMP and **(c)** P.OMZ parameterizations.

BGD
11, 16703–16742, 2014

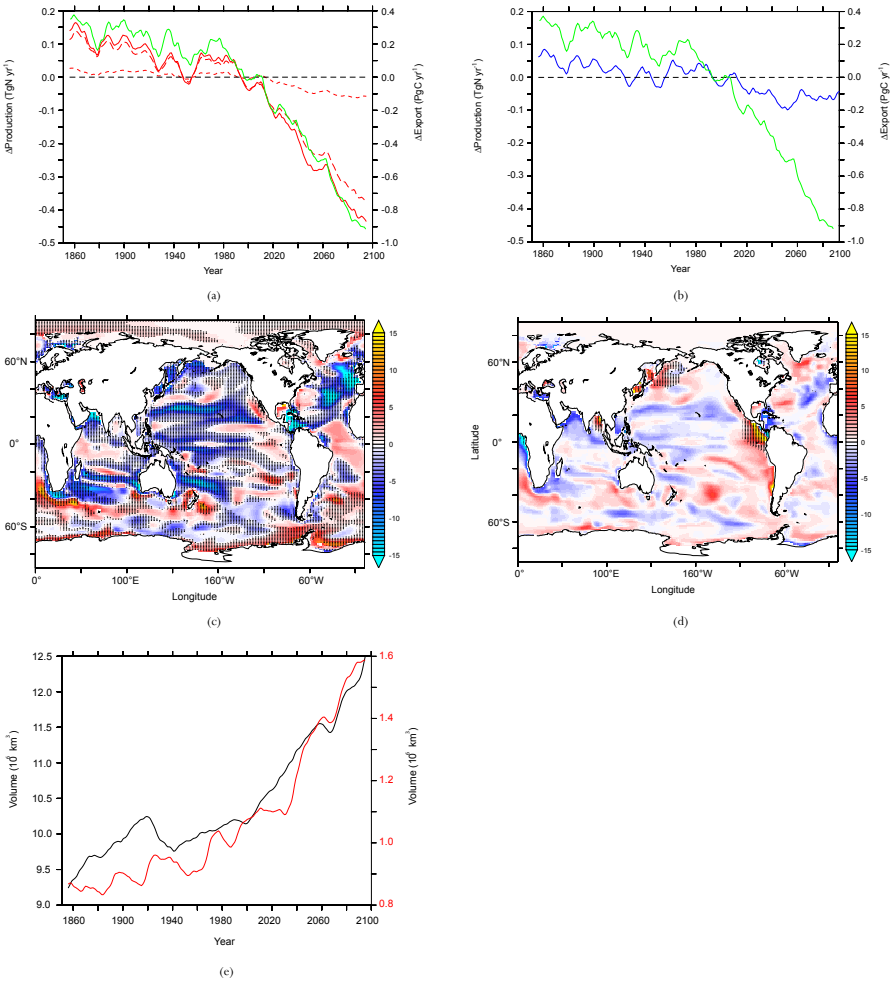

BGD
11, 16703–16742, 2014

Oceanic N_2O emissions in the 21st century

J. Martinez-Rey et al.

Figure 5. (a) Anomalies in export of organic matter at 100 m (green), low-O_2 production pathway (short dashed red), high-O_2 production pathway (long dashed red) and total P.OMZ production (red) from 1851 to 2100 using the historical and future RCP8.5 simulations. **(b)** Anomalies in export of organic matter at 100 m (green) and P.TEMP production (blue) over the same time period. **(c)** Change in high-O_2 production pathway of N_2O (in mg N m^{-2} yr^{-1}) in the upper 1500 m between 2080–2100 to 1985–2005 averaged time periods. Hatched areas indicate regions where change in export of organic matter at 100 m deep have the same sign as in changes in high-O_2 production pathway. **(d)** Change in low-O_2 production pathway of N_2O (in mg N m^{-2} yr^{-1}) in the upper 1500 m between 2080–2100 to 1985–2005 averaged time periods. Hatched areas indicate regions where oxygen minimum zones ($O_2 < 5$ µmol L^{-1}) expand. **(e)** Volume (in 10^6 km^3) of hypoxic (black, $O_2 < 60$ µmol L^{-1}) and suboxic (red, $O_2 < 5$ µmol L^{-1}) areas in the 1851 to 2100 period in NEMO-PISCES historical and future RCP8.5 simulations.

BGD
11, 16703–16742, 2014

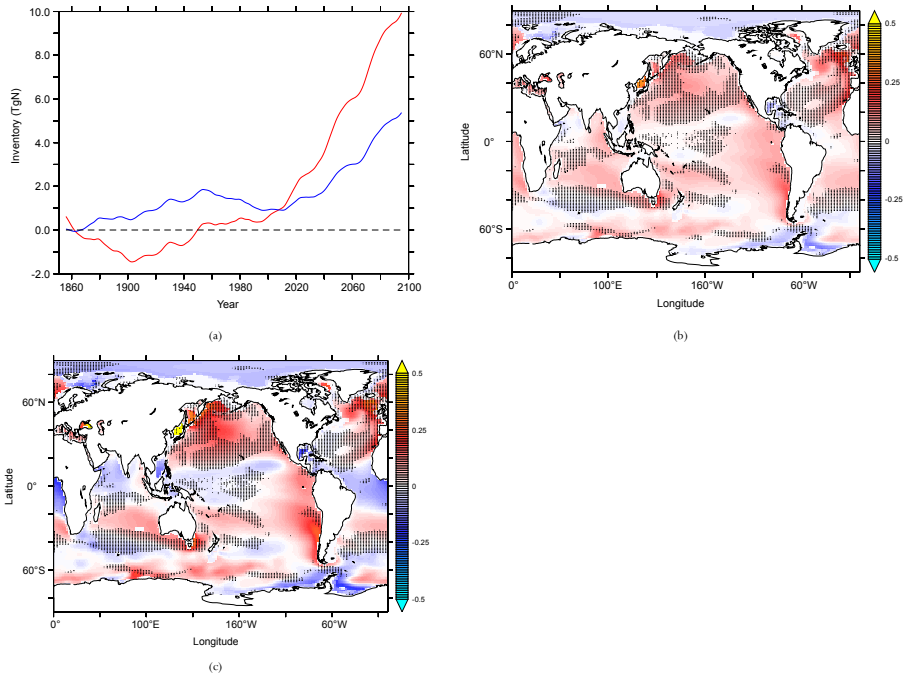

Figure 6. (a) Anomalies in N_2O inventory (in Tg N) from 1851 to 2100 in P.TEMP (blue) and P.OMZ (red) using the historical and future RCP8.5 simulations in the upper 1500 m. Change in vertically integrated N_2O concentration (in mg N m^{-2}) in the upper 1500 m using NEMO-PISCES model mean from the averaged 2080–2100 to 1985–2005 time periods in future RCP8.5 and historical scenarios respectively in **(b)** P.TEMP and **(c)** P.OMZ. Hatched areas indicate regions where mixed layer depth is reduced by more than 5 m in 2080–2100 compared to 1985–2005.

BGD
11, 16703–16742, 2014

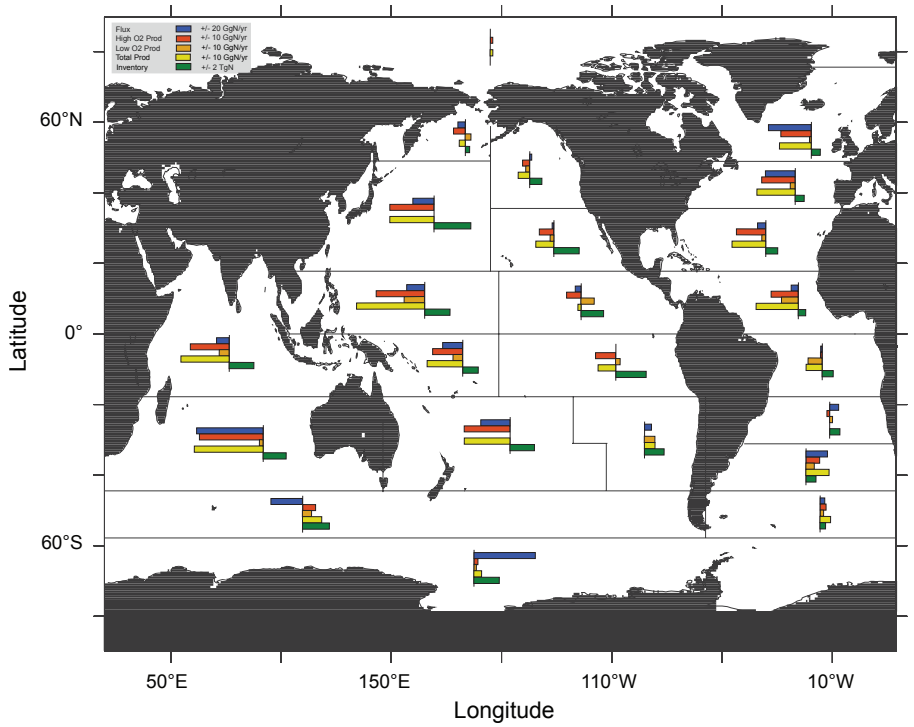

Figure 7. Change in the whole water column in N_2O sea-to-air flux (blue), high-O_2 production pathway (red), low-O_2 production pathway (orange), total N_2O production (yellow) and N_2O inventory (green) for P.OMZ from the averaged 2080–2100 to present 1985–2005 averaged time period in the NEMO-PISCES historical and future RCP8.5 simulations (based on Mikaloff-Fletcher et al. (2006) oceanic regions).

BGD
11, 16703–16742, 2014

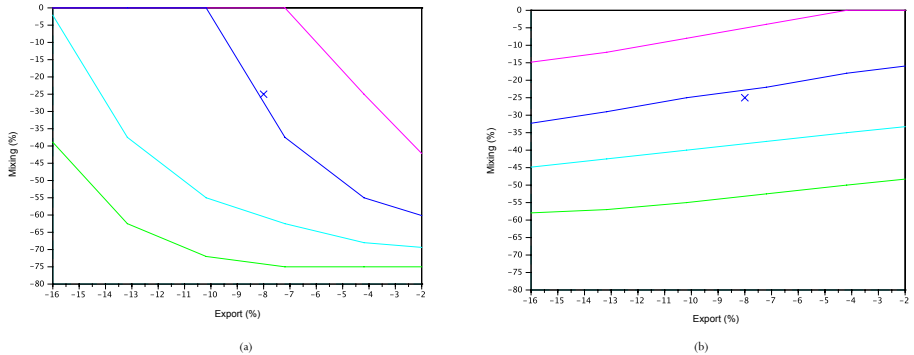

Figure 8. Constant regimes of **(a)** N_2O sea-to-air flux (in percentage of the historical flux: 95 % pink, 90 % blue, 85 % cyan and 80 % green) and **(b)** N_2O concentration in the deep (in percentage of the historical concentration: 90 % pink, 110 % blue, 125 % cyan and 150 % green) in 2100 as a result of a reduction in the export coefficient ε (in %) and in the mixing coefficient μ (in %) in the box model.

BGD
11, 16703–16742, 2014